A FAS Approach for Robust Trajectory Tracking Control of a 3-DOF Quadrotor

Junxiang Zhang[1], Weijie Ren[1], Yulin Duan[1], Guang-Ren Duan[1,2,*]

1. Guangdong Provincial Key Laboratory of Fully Actuated System Control Theory and Technology, Southern University of Science and Technology, Shenzhen 518055, P. R. China
E-mail: zjunxiang960@gmail.com,weijie.ren@outlook.com,duan_yu_lin@163.com

2. Center for Control Theory and Guidance Technology, Harbin Institute of Technology, Harbin 150001, P. R. China
E-mail: g.r.duan@hit.edu.cn, duangr@sustech.edu.cn

Abstract: This paper proposes a quadrotor control strategy based on the fully actuated system (FAS) approach, aiming to enhance trajectory tracking robustness under external disturbances. By establishing the dynamic model of a three-degree-of-freedom (3-DOF) planar quadrotor system, we develop a controller by the FAS approach that analytically computes input derivatives and integrates a novel robust compensator to mitigate high-order disturbances. The proposed method eliminates the need for designing extended observers to estimate the higher-order derivatives of the input, thereby simplifying the system structure and avoiding the cumulative estimation errors observed in conventional approaches. Theoretical contributions include a Lyapunov-based stability proof demonstrating bounded convergence of tracking errors into an ellipsoidal region centered at the origin. Simulation results validate the framework's effectiveness. The method demonstrates practical significance through its ability to maintain physically realizable control inputs while handling bounded disturbances. This work provides direct implications for applications requiring precise trajectory tracking in adverse conditions.

Key Words: Fully actuated system approach, 3-DOF quadrotor, robust control, trajectory tracking

1 Introduction

In recent decades, quadrotors have emerged as a critical platform in robotics research due to their unique capabilities in vertical take-off, landing, and agile maneuvering, enabled by their simple mechanical design compared to traditional rotorcraft [1]. However, the underactuated nature of these systems, where four rotor inputs are used to control six degrees of freedom (comprising 3-DOF translational position and 3-DOF orientation), presents significant challenges for precise trajectory tracking and effective disturbance rejection [2]. Traditional hierarchical control architectures, which decouple attitude and position dynamics into separate loops, often fail to address the coupling effects and high-order nonlinearities inherent in quadrotor systems [3]. While linear PID controllers and nonlinear methods like sliding mode control (SMC) have shown partial success [4], [5], their reliance on simplified dynamics or high-gain switching limits their robustness in practical scenarios. Recent advancements in fully actuated system (FAS) modeling provide a transformative framework for quadrotor control by directly canceling nonlinearities through full actuation, enabling globally stabilized linear subsystems [6], [7]. Unlike hierarchical designs, the fully actuated system approach avoids the assumption of time-scale separation between attitude and position dynamics, offering a unified control structure. [8] focuses on predictive path-following control for a tilt-quadrotor UAV based on fully-actuated system approaches, demonstrating the versatility of FAS in handling advanced aerial platforms.

Nevertheless, a critical limitation arises for certain nonlinear systems, such as quadrotors, since they cannot be transformed into the pseudo strict-feedback form, which is a structural prerequisite for conventional FAS frameworks [7]. To address this challenge, we adopt a modified FAS methodology proposed in [1], which circumvents the need for strict-feedback representation while retaining the advantages of full actuation. However, a critical limitation of existing FAS implementations lies in handling high-order unmeasurable terms, such as input derivatives $\dot{u}_1$, $\ddot{u}_1$ and disturbance derivatives. Previous works, such as [3], address this by designing extended state observers (ESOs) to estimate these terms. While effective, observer-based approaches introduce additional complexity and tuning requirements, and the estimation errors of observers(especially for high-order terms) can degrade control performance. The statistical frameworks in [9] and [10], which derive jerk dynamics from white noise-driven processes, produce estimators that exhibit no intrinsic distinction from second-order low-pass filters in their fundamental operational principles. Furthermore, while differential flatness-based formulations [11], [12], successfully establish algebraic relationships between jerk and angular velocity/acceleration for idealized models, these methods systematically omit input derivative terms Moreover, robust control of nonlinear systems remains an open challenge, particularly in the presence of high-order disturbances and model uncertainties. Recent work by [13] has made significant progress in this area by proposing a novel robust control framework that explicitly addresses high-order disturbances. Inspired by this approach, our work extends the FAS framework to incorporate robust control techniques for handling high-order disturbances, while directly computing input derivatives to avoid the complexities and estimation errors of observer design. In this paper, we propose a novel FAS-based control strategy for a 3-DOF pla-

*Corresponding author. This work was supported by the Science Center Program of the National Natural Science Foundation of China (NSFC) under Grant No. 62188101 and the NSFC under Grant No. 623B2045. This work was also supported by the Guangdong Provincial Key Laboratory of Fully Actuated System Control Theory and Technology (2024B1212010002), the Shenzhen Science and Technology Program under Grant No. KQTD20221101093557010, as well as the Special Funds for the Cultivation of Guangdong College Students' Scientific and Technological Innovation ("Climbing Program" Special Funds) under funding No. pdjh2025c11603.

nar quadrotor system that focuses on two translational degrees of freedom (horizontal and vertical motion) and one rotational degree of freedom (pitch angle). Our key contributions are as follows:

1) Unlike [3], which relies on ESOs to estimate high-order terms, our method analytically computes input derivatives $\dot{u}_1$, $\ddot{u}_1$ from the system model, avoiding observer design complexities and eliminating estimation errors.
2) Building on the framework proposed in [13], we integrate a robust control mechanism into the FAS framework to explicitly handle high-order disturbances and model uncertainties, ensuring stable and accurate tracking performance.

The remainder of this paper is organized as follows. Section II introduces essential preliminaries, including unified mathematical notations and the theoretical foundation of the fully actuated system framework. Section III establishes the 3-DOF planar quadrotor dynamic model with disturbance considerations. Section IV presents the FAS controller design and provides rigorous Lyapunov-based stability proofs for the closed-loop system. Section V validates the proposed method through comparative MATLAB simulations. Finally, Section VI concludes with practical insights and future research directions.

2 Preliminaries

2.1 Notations

In this article, we adopt the following notations: $\mathbb{R}$ denotes the set of real numbers, $\mathbb{R}^n$ represents the n-dimensional real vector space, $\mathbb{R}^{m\times n}$ denotes the space of $m\times n$ real matrices, and I_n represents the n-th order identity matrix.

Additionally, for $x \in \mathbb{R}^m$ and matrices $A_i \in \mathbb{R}^{m\times m}$ where $i = 1, 2, \ldots, n$, the following symbols are frequently used throughout the paper:

$$x^{(0\sim m)} \triangleq \begin{bmatrix} x^\top & \dot{x}^\top & \cdots & \left(x^{(m)}\right)^\top \end{bmatrix}^\top,$$
$$A_{0\sim m} \triangleq \begin{bmatrix} A_0 & A_1 & \cdots & A_m \end{bmatrix},$$
$$\Phi\left(A_{0\sim n}\right) = \begin{bmatrix} 0 & I & & \\ & & \ddots & \\ & & & I \\ -A_0 & -A_1 & \cdots & -A_n \end{bmatrix}.$$

2.2 FAS model

In [13], for some nonlinear systems subject to uncertainties, their FAS models can be derived in the following form:

$$x^{(n)} = f\left(x^{(0\sim n-1)}\right) + \Delta f\left(x^{(0\sim n-1)}\right) + L\left(x^{(0\sim n-1)}\right) u,$$

where $x, u \in \mathbb{R}^r$ are the state vector and the control input vector, respectively, $f\left(x^{(0\sim n-1)}\right) \in \mathbb{R}^r$ is a continuous vector function, $L\left(x^{(0\sim n-1)}\right) \in \mathbb{R}^{r\times r}$ is a continuous matrix function satisfying the following conditions, and $\Delta f\left(x^{(0\sim n-1)}\right) \in \mathbb{R}^n$ is the nonlinear uncertainty of the system. $L\left(x^{(0\sim n-1)}\right)$ satisfies the following assumption:

Assumption 1 *The matrix $L\left(x^{(0\sim n-1)}\right)$, which represents the control gain, satisfies the following full-ctuation assumption for all $x^{(0\sim n-1)} \in \mathbb{R}^{nr}$,*

$$\det L\left(x^{(0\sim n-1)}\right) \neq 0.$$

3 3-DOF Quadrotor Model

A schematic representation of this system is illustrated in Fig. 1. The quadrotor is constrained to move within the x-z plane.

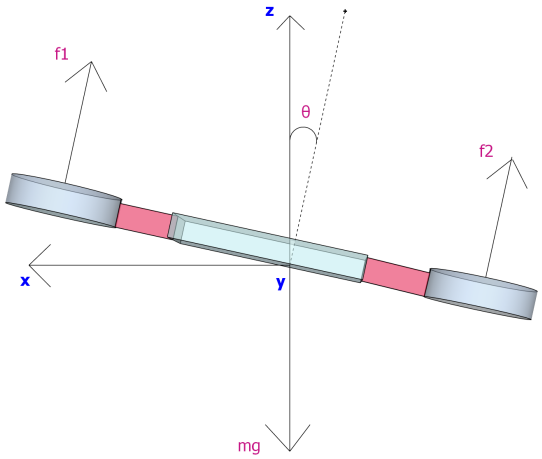

Fig. 1: 3-DOF quadrotor for a planar motion.

Consider the following 3-DOF planar quadrotor system [14], which describes the dynamics of the quadrotor in a planar motion. The system is governed by the following set of equations, where f_1 and f_2 represent the forces generated by the rotors, m is the mass of the quadrotor, J is the moment of inertia, g is the gravitational acceleration, θ is the pitch angle, and d_1, d_2, d_3 denote external time-varying disturbances:

$$\begin{cases} \ddot{x} = \frac{f_1+f_2}{m}\sin\theta + d_1, \\ \ddot{z} = \frac{f_1+f_2}{m}\cos\theta - g + d_2, \\ \ddot{\theta} = \frac{f_2-f_1}{J} + d_3. \end{cases} \tag{1}$$

To simplify the control design, the system dynamics can be reformulated in terms of control inputs u_1 and u_2, where $u_1 = \frac{f_1+f_2}{m}$ represents the total thrust force normalized by the mass, and $u_2 = \frac{f_2-f_1}{J}$ represents the normalized torque. The reformulated dynamics is given by:

$$\begin{cases} \ddot{x} = u_1\sin\theta + d_1, \\ \ddot{z} = u_1\cos\theta - g + d_2, \\ \ddot{\theta} = u_2 + d_3. \end{cases} \tag{2}$$

We define Δz and Δx as follows, which will be frequently used throughout the rest of the article.

$$\begin{cases} \Delta z = z - z^*, \\ \Delta x = x - x^*. \end{cases} \tag{3}$$

Here, z^* and x^* denote the reference signals for z and x, respectively.

Assumption 2 *To facilitate the control design and ensure the stability of the system, the following assumptions are*

made:

$$\begin{cases} |\theta| < \frac{\pi}{2}, \\ |\ddot{d}_1(t) + (u_1 \cos\theta + R_1 \tan^2\theta) d_3(t)| \leq \rho_1, \\ |d_2(t)| \leq \rho_2, \\ |u_1| \leq 50\,\mathrm{N}, \\ |u_2| \leq 50\,\mathrm{N}, \\ -R_1 \tan^2\theta - u_1 \cos\theta \neq 0. \end{cases} \tag{4}$$

Here, ρ_1 and ρ_2 are two positive scalars representing the bounds of the disturbances.

Remark 1: The pitch angle θ is restricted to $|\theta| < \frac{\pi}{2}$ to avoid singularities in the control law and ensure the quadrotor remains within a physically achievable orientation range. In practical applications, even approaching $\theta = \frac{\pi}{2}$ is generally not permissible due to the risk of lossing control authority. The control inputs u_1 and u_2 are bounded by 50 N, reflecting the physical limitations of the maximum thrust and torque. The disturbances d_1 and d_2 are assumed to be bounded, which is a reasonable assumption for external forces such as wind gusts or payload variations. The assumption $-R_1 \tan^2\theta - u_1 \cos\theta \neq 0$ ensures the non-singularity of the control law and is essential for the stability of the system.

4 Controller Design and Robustness Analysis

The system can be decomposed into two subsystems, for which controllers are designed separately.

4.1 Controller Design for Subsystem I

The first subsystem dynamics is governed by

$$\ddot{z} = u_1 \cos\theta - g + d_2. \tag{5}$$

The control input u_1 is designed as

$$u_1 = \frac{R_1}{\cos\theta}, \tag{6}$$

where R_1 takes the form:

$$\begin{aligned} R_1 = {} & g - A^z_{0\sim1} z^{(0\sim1)} - \frac{1}{4\varepsilon} {\rho_2}^2 P_{L2}^{\top} \left(A^z_{0\sim1}\right) z^{(0\sim1)} \\ & + \dddot{z}^* + A^z_{0\sim1} z^{*(0\sim1)} + \frac{1}{4\varepsilon} {\rho_2}^2 P_{L2}^{\top} \left(A^z_{0\sim1}\right) z^{*(0\sim1)}. \end{aligned} \tag{7}$$

Here, $P_{L2} \in \mathbb{R}^{2\times1}$ and ε is an arbitrarily given positive number.

Substituting (6) into (5) yields the closed-loop dynamics:

$$\Delta\ddot{z} + A^z_{0\sim1} \Delta z^{(0\sim1)} = \phi(z^{(0\sim1)}), \tag{8}$$

with $\phi(z^{(0\sim1)})$ defined by

$$\phi(z^{(0\sim1)}) = -\frac{1}{4\varepsilon} {\rho_2}^2 P_{L2}^{\top} \left(A^z_{0\sim1}\right) \Delta z^{(0\sim1)} + d_2. \tag{9}$$

4.2 Controller Design for Subsystem II

The dynamics of the second subsystem is characterized by:

$$\ddot{x} = u_1 \sin\theta + d_1. \tag{10}$$

Taking the first time derivative of (10) yields

$$\dddot{x} = \dot{u}_1 \sin\theta + u_1 \dot{\theta} \cos\theta + \dot{d}_1. \tag{11}$$

Subsequently, differentiating (11) with respect to time produces

$$x^{(4)} = \ddot{u}_1 \sin\theta + R_2 + u_2 u_1 \cos\theta + d_3 u_1 \cos\theta + \ddot{d}_1, \tag{12}$$

where the intermediate term R_2 is defined as

$$R_2 = 2\dot{u}_1 \dot{\theta} \cos\theta - \dot{\theta}^2 u_1 \sin\theta. \tag{13}$$

It is noteworthy that $\dot{u}_1$ and $\ddot{u}_1$ emerge in the preceding equations. These derivatives can be systematically computed through the following expressions. The first derivative of u_1 is given by:

$$\dot{u}_1 = \frac{\dot{R}_1 \cos\theta + R_1 \dot{\theta} \sin\theta}{\cos^2\theta}, \tag{14}$$

Building upon this result, the second derivative of u_1 is derived as:

$$\begin{aligned} \ddot{u}_1 = {} & \frac{\ddot{R}_1 \cos\theta + R_1(\dot{\theta}^2 \cos\theta + \ddot{\theta} \sin\theta)}{\cos^2\theta} \\ & + \frac{2\dot{\theta} \sin\theta (\dot{R}_1 \cos\theta + R_1 \dot{\theta} \sin\theta)}{\cos^3\theta}. \end{aligned} \tag{15}$$

By substituting the third equation of (2) into the above expression, we obtain

$$\begin{aligned} \ddot{u}_1 = {} & \frac{\ddot{R}_1 \cos\theta + R_1(\dot{\theta}^2 \cos\theta + (u_2 + d_3) \sin\theta)}{\cos^2\theta} \\ & + \frac{2\dot{\theta} \sin\theta (\dot{R}_1 \cos\theta + R_1 \dot{\theta} \sin\theta)}{\cos^3\theta}. \end{aligned} \tag{16}$$

The required derivatives $\dot{R}_1$ and $\ddot{R}_1$ are obtained from:

$$\begin{cases} \dot{R}_1 = -A^z_{0\sim1} z^{(1\sim2)} - \frac{1}{4\varepsilon} \rho_2^2 P_{L2}^{\mathsf{T}} (A^z_{0\sim1}) z^{(1\sim2)} \\ \qquad + \dddot{z}^* + A^z_{0\sim1} z^{*(1\sim2)} + \frac{1}{4\varepsilon} \rho_2^2 P_{L2}^{\mathsf{T}} (A^z_{0\sim1}) z^{*(1\sim2)}, \\ \ddot{R}_1 = -A^z_{0\sim1} z^{(2\sim3)} - \frac{1}{4\varepsilon} \rho_2^2 P_{L2}^{\mathsf{T}} (A^z_{0\sim1}) z^{(2\sim3)} \\ \qquad + z^{*(4)} + A^z_{0\sim1} z^{*(2\sim3)} + \frac{1}{4\varepsilon} \rho_2^2 P_{L2}^{\mathsf{T}} (A^z_{0\sim1}) z^{*(2\sim3)}, \end{cases} \tag{17}$$

Observing that u_2 appears explicitly in the expression for $\ddot{u}_1$, considering both (12) and (16), we can obtain:

$$u_2 = \frac{R_3}{-R_1 \tan^2\theta - u_1 \cos\theta}, \tag{18}$$

where the intermediate term R_3 is given by:

$$\begin{aligned} R_3 = {} & R_2 + A^x_{0\sim3} x^{(0\sim3)} - A^x_{0\sim3} x^{*(0\sim3)} - x^{*(4)} \\ & + \frac{1}{4\varepsilon} \rho_1^2 P_{L1}^{\mathsf{T}} (A^x_{0\sim3}) x^{(0\sim3)} - \frac{1}{4\varepsilon} \rho_1^2 P_{L1}^{\mathsf{T}} (A^x_{0\sim3}) x^{*(0\sim3)} \\ & + \frac{(\ddot{R}_1 \cos\theta + R_1 \dot{\theta}^2 \cos\theta) \sin\theta}{\cos^2\theta} \\ & + \frac{2\dot{\theta} \sin\theta (\dot{R}_1 \cos\theta + R_1 \dot{\theta} \sin\theta)}{\cos^3\theta}. \end{aligned} \tag{19}$$

Here, P_{L1} is a given matrix in $\mathbb{R}^{4\times1}$.

Substituting (18) into (10) yields the closed-loop dynamics:

$$\Delta x^{(4)} + A^x_{0\sim3} \Delta x^{(0\sim3)} = \phi(x^{(0\sim3)}) \ , \tag{20}$$

where $\phi^{(0\sim3)}$ is defined as

$$\begin{aligned}\phi(x^{(0\sim3)}) = &-\frac{1}{4\varepsilon}\rho_1^2 P_{L1}^{\mathsf{T}}(A^x_{0\sim3})\Delta x^{(0\sim3)} \\ &+\left(-R_1\tan^2\theta + u_1\cos\theta\right)d_3 + \ddot{d}_1.\end{aligned} \tag{21}$$

Theorem 1 *If the control inputs u_1 and u_2 are designed as (6) and (18) , then it can be guaranteed that $\Delta z^{0\sim1}$ and $\Delta x^{0\sim3}$ converge into the following ellipsoid centered at the origin:*

$$\Theta_{\mu,\varepsilon}(0) = \left\{x^{(0\sim n-1)} \,\middle|\, \left(x^{(0\sim n-1)}\right)^\top P\left(A^{0\sim n-1}\right)x^{(0\sim n-1)} \le \tfrac{\varepsilon}{\mu}\right\},$$

where μ is a positive number.

The detailed proof will be presented in the subsequent part.

Proof:

To prove the theorem, some useful lemmas are given here.

Lemma 1 *[13] Let a and b be two real numbers, and $b > 0$. Then the following relation holds:*

$$a - \frac{a^2}{4b} \leqslant b. \tag{22}$$

Lemma 2 *[6] For an arbitrarily selected $F \in \mathbb{R}^{mn\times mn}$, all the matrices $A_{0\sim m-1}$ and the nonsingular matrix $V \in \mathbb{R}^{mn\times mn}$ satisfying*

$$\Phi(A_{0\sim m-1}) = VFV^{-1}$$

are given by

$$A_{0\sim m-1} = -ZF^nV^{-1}(Z,F), \tag{23}$$

$$V = V(Z,F) = \begin{bmatrix} Z \\ ZF \\ ZF^2 \\ \vdots \\ ZF^{n-1}\end{bmatrix}, \tag{24}$$

where $Z \in \mathbb{R}^{m\times mn}$ is an arbitrary parameter matrix satisfying

$$\det V(Z,F) \neq 0. \tag{25}$$

According to (23), the parametric matrices $A_{0\sim m-1}$ can be directly computed by choosing an arbitrary matrix Z, as long as (25) is not violated.

Condition 1

$$\mathrm{Re}\lambda_i\left(\Phi\left(A^{0\sim n-1}\right)\right) < -\frac{\mu}{2}, \quad i = 1,2,\ldots,nr.$$

The closed-loop system (8) can be written in the following state-space form:

$$\Delta\dot{z}^{(0\sim1)} = \Phi(A^z_{0\sim1})\Delta z^{(0\sim1)} + \begin{bmatrix}0\\ \phi(z^{(0\sim1)})\end{bmatrix}. \tag{26}$$

If we select a matrix F satisfying

$$\mathrm{Re}\lambda_i(F) < -\frac{\mu}{2}, \quad i = 1,2,\ldots,nr. \tag{27}$$

Then $A_i \in \mathbb{R}^{r\times r}, i = 0,1,\ldots,n-1$ satisfy the Condition 1 [13], there exists a positive definite matrix $P(A^{0\sim n-1})$ satisfying

$$\Phi^\top(A^z_{0\sim1})P + P\Phi(A^z_{0\sim1}) \le -\mu P. \tag{28}$$

Partition P as

$$P = \begin{bmatrix}P_1 & P_2 & \cdots & P_n\end{bmatrix}, \quad P_i \in \mathbb{R}^{nr\times r}, \tag{29}$$

where P_i represents the i-th block of the partitioned matrix. We can further introduce the following notation, which will be used in the paper:

$$P_L = P\begin{bmatrix}0\\ I_r\end{bmatrix} = P_n. \tag{30}$$

Then the following Lyapunov function can be chosen for the system (8) and (20):

$$V_z = \frac{1}{2}\left(\Delta z^{(0\sim1)}\right)^\top P(A^z_{0\sim1})\Delta z^{(0\sim1)}, \tag{31}$$

$$V_x = \frac{1}{2}\left(\Delta x^{(0\sim3)}\right)^\top P(A^x_{0\sim3})\Delta x^{(0\sim3)}. \tag{32}$$

In view of (8), (28), (30) and Lemma 1, we have

$$\begin{aligned}\dot{V}_z &= \frac{1}{2}\Delta\dot{z}^\top P\Delta z + \frac{1}{2}\Delta z^\top P\Delta\dot{z} \\ &= \frac{1}{2}\left(\Phi\Delta z^{(0\sim1)} + \begin{bmatrix}0\\ \phi(z^{(0\sim1)})\end{bmatrix}\right)^\top P\Delta z^{(0\sim1)} \\ &\quad + \frac{1}{2}\left(\Delta z^{(0\sim1)}\right)^\top P\left(\Phi\Delta z^{(0\sim1)} + \begin{bmatrix}0\\ \phi(z^{(0\sim1)})\end{bmatrix}\right) \\ &= \frac{1}{2}\left(\Delta z^{(0\sim1)}\right)^\top\left(\Phi^\top P + P\Phi\right)\Delta z^{(0\sim1)} \\ &\quad + \left(\Delta z^{(0\sim1)}\right)^\top P\begin{bmatrix}0\\ \phi(z^{(0\sim1)})\end{bmatrix} \\ &\le -\frac{\mu}{2}\left(\Delta z^{(0\sim1)}\right)^\top P\Delta z^{(0\sim1)} \\ &\quad + \left(\Delta z^{(0\sim1)}\right)^\top P_L\phi(\Delta z^{(0\sim1)}) \\ &= -\mu V_z + \left(\Delta z^{(0\sim1)}\right)^\top P_L\phi(z^{(0\sim1)}).\end{aligned}$$

Next, let us consider the last term of the above equation. It follows from Condition 1, Lemma 1and Equation (9) that

$$\begin{aligned}&\left(\Delta z^{(0\sim1)}\right)^\top P_L\phi(z^{(0\sim1)}) \\ &= -\frac{{\rho_2}^2\left(\Delta z^{(0\sim1)}\right)^\top P_L P_L^\top\Delta z^{(0\sim1)}}{4\varepsilon} + \left(\Delta z^{(0\sim1)}\right)^\top P_L d_2 \\ &= -\frac{{\rho_2}^2\left\|P_L^\top\Delta z^{(0\sim1)}\right\|^2}{4\varepsilon} + \left(\Delta z^{(0\sim1)}\right)^\top P_L d_2 \\ &\le \frac{{\rho_2}^2\left\|P_L^\top\Delta z^{(0\sim1)}\right\|^2}{4\varepsilon} + \|d_2\|\left\|P_L^\top\Delta z^{(0\sim1)}\right\| \\ &\le \frac{{\rho_2}^2\left\|P_L^\top\Delta z^{(0\sim1)}\right\|^2}{4\varepsilon} + \rho_2\left\|P_L^\top\Delta z^{(0\sim1)}\right\| \\ &\le \varepsilon.\end{aligned}$$

Combining the above two equations gives

$$\dot{V}_z \leq -\mu V_z + \varepsilon. \tag{33}$$

It thus follows from the Comparison Theorem that

$$V_z \leq V_z(0)e^{-\mu t} + \frac{\varepsilon}{\mu}\left(1 - e^{-\mu t}\right), \tag{34}$$

which gives

$$V_z \leq \left(V_z(0) - \frac{\varepsilon}{\mu}\right)e^{-\mu t} + \frac{\varepsilon}{\mu} \to \frac{\varepsilon}{\mu}, \quad t \to \infty. \tag{35}$$

Thus $\Delta z^{(0\sim1)}$ eventually converges into the ellipsoid $\Theta_{\mu,\varepsilon}(0)$. We can also prove $\Delta x^{(0\sim3)}$ eventually converges into the ellipsoid $\Theta_{\mu,\varepsilon}(0)$ in the same way. The proof is then completed. ■

5 Simulation

This section demonstrates the MATLAB simulation results to validate the proposed FAS approach for robust trajectory tracking control of a 3-DOF quadrotor system.

The key system parameters are configured as follows: the mass of the quadrotor is set to $m = 1.0\,\mathrm{kg}$, the moment of inertia is $J = 0.01\,\mathrm{kg}\cdot\mathrm{m}^2$, and the gravitational acceleration is $g = 9.8\,\mathrm{m/s}^2$. The disturbances d_1, d_2, d_3 and corresponding bounds ρ_1, ρ_2 are listed below:

$$\begin{cases} d_1 = 0.02\sin(\pi t)\,\mathrm{N/kg}, \\ d_2 = 0.02\sin(\pi t)\,\mathrm{N/kg}, \\ d_3 = 0.02\sin(\pi t)\,\mathrm{N/kg}, \\ \rho_1 = 0.2, \\ \rho_2 = 0.02. \end{cases}$$

Then we can select $\varepsilon = 10^{-5}$ to complete the robust controller synthesis. To satisfy Condition 1, the control parameters are selected as:

$$\begin{aligned} F_1 &= \mathrm{diag}\left(\begin{bmatrix}-10 & -15 & -20 & -25\end{bmatrix}\right), \\ Z_1 &= \begin{bmatrix}1 & 1 & 1 & 1\end{bmatrix}, \\ F_2 &= \mathrm{diag}\left(\begin{bmatrix}-10 & -15\end{bmatrix}\right), \\ Z_2 &= \begin{bmatrix}1 & 1\end{bmatrix}. \end{aligned}$$

Following Lemma 2, the controller gains are obtained as:

$$\begin{aligned} A^x_{0\sim3} &= \begin{bmatrix}7.5 & 19.25 & 17.75 & 7\end{bmatrix}, \\ A^z_{0\sim1} &= \begin{bmatrix}1.5 & 2.5\end{bmatrix}. \end{aligned}$$

The reference trajectories are defined by:

$$\begin{cases} x^* = \sin(t)\,\mathrm{m}, \\ z^* = \cos(t)\,\mathrm{m}. \end{cases}$$

The performance of the proposed control strategy is evaluated through simulations, and the results are presented in Figs. 2–5.

The states x, z with and without the robust compensator are illustrated in Fig. 2. It is evident that the proposed method achieves significantly better tracking of the reference

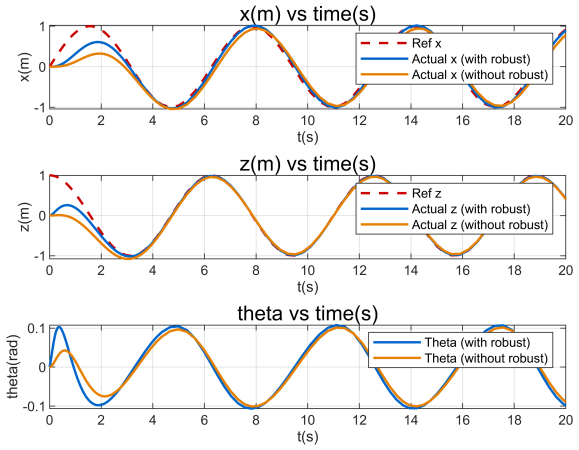

Fig. 2: Reference and actual states for x, z, and θ with and without robust compensator.

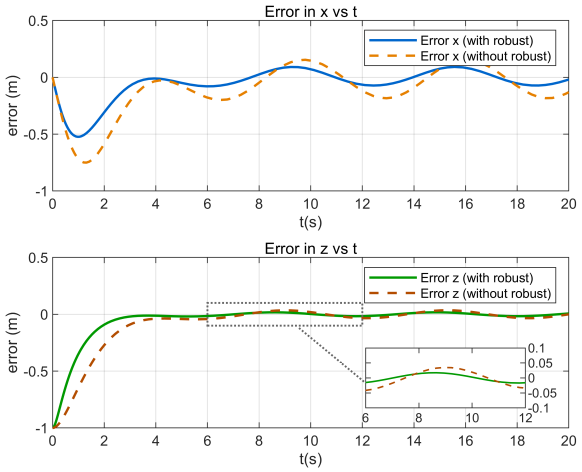

Fig. 3: Errors in x and z with and without robust compensator.

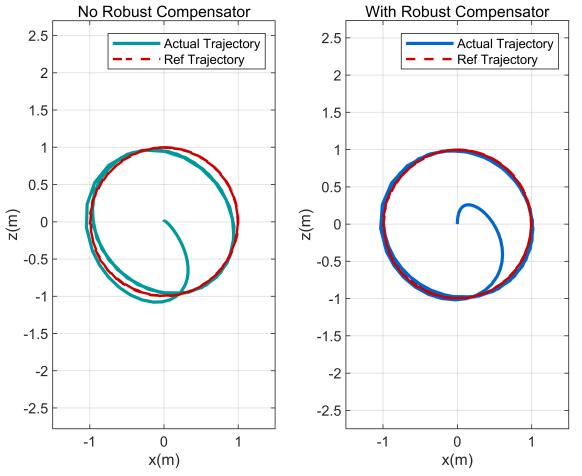

Fig. 4: Trajectory comparison with and without robust compensator.

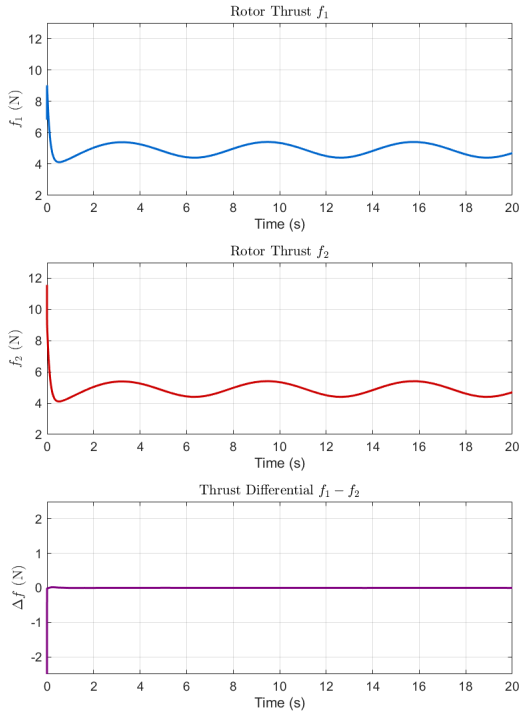

Fig. 5: Rotor thrusts f_1 and f_2.

trajectories in the presence of disturbances. The robust compensator effectively mitigates the impact of external disturbances, ensuring more accurate state trajectories.

The errors in x and z relative to the reference over time are shown in Fig. 3. Compared to the basic FAS method without robust control, the maximum errors in x and z are reduced by **40.9%** and **53.0%**, respectively, when the robust compensator is used. This substantial reduction highlights the effectiveness of the proposed method in improving the tracking precision under disturbances.

Fig. 4 compares the deviations of the trajectory with and without robust control, demonstrating that the robust compensator significantly reduces the deviations of the desired trajectory, particularly during transient phases and in the presence of disturbances.

Fig. 5 displays the time-varying rotor thrusts f_1 and f_2. In particular, the difference between the thrusts of the rotors, $\Delta f = f_1 - f_2$, is also plotted. It is observed that Δf exhibits a brief transient fluctuation at the initial stage but quickly stabilizes to zero, indicating that the control inputs are well-balanced and the system achieves steady-state performance efficiently.

6 Conclusion

This paper developed a robust control strategy based on the FAS approach for 3-DOF quadrotor trajectory tracking. By directly computing high-order input derivatives within the FAS framework, the proposed method eliminates observer dependency while explicitly compensating for disturbances through Lyapunov-based robust terms. Theoretical analysis guarantees bounded-error convergence, with simulations demonstrating **40.9%** and **53.0%** reductions in tracking errors compared to non-robust baselines. Future work will extend this approach to 6-DOF quadrotor systems and experimental implementations, and the interval observer technique [15] will also be considered to reconstruct the state bound of quadrotors.

References

[1] S. Lu, K. Tsakalis, and Y. Chen, Development and application of a novel high-order fully actuated system approach—Part I: 3-DOF quadrotor control. *IEEE Control Systems Letters*, 2022, 7: 1177–1182.

[2] T. Chen and J. Shan, Quadrotor control based on a high-order system model, in *Proceedings of AIAA SCITECH 2022 Forum*, 2022: 1143.

[3] S. Lu, K. Tsakalis, and Y. Chen, High-order fully actuated system approach for a 3-DOF quadrotor control based on extended state observers, in *Proceedings of 2024 3rd Conference on Fully Actuated System Theory and Applications (FASTA)*, 2024: 1555–1560.

[4] J. Li and Y. Li, Dynamic analysis and PID control for a quadrotor, in *Proceedings of 2011 IEEE International Conference on Mechatronics and Automation*, 2011: 573–578.

[5] F. Chen, R. Jiang, K. Zhang, B. Jiang, and G. Tao, Robust backstepping sliding-mode control and observer-based fault estimation for a quadrotor UAV. *IEEE Transactions on Industrial Electronics*, 2016, 63(8): 5044–5056.

[6] G. R. Duan, High-order fully actuated system approaches: Part I. Models and basic procedure. *International Journal of Systems Science*, 2021, 52(2): 422–435.

[7] G. R. Duan, High-order fully actuated system approaches: Part II. Generalized strict-feedback systems. *International Journal of Systems Science*, 2021, 52(3): 437–454.

[8] L. Xu, X. Wang, P. He, and Y. Wang, Predictive path-following control for tilt-quadrotor UAV based on fully-actuated system approaches, in *Proceedings of 2024 3rd Conference on Fully Actuated System Theory and Applications (FASTA)*, 2024: 1382–1387.

[9] W. Xu, D. He, Y. Cai, and F. Zhang, Robots' state estimation and observability analysis based on statistical motion models. *IEEE Transactions on Control Systems Technology*, 2022, 30(5): 2030–2045.

[10] S. Nakazawa, T. Ishihara, and H. Inooka, Real-time algorithms for estimating jerk signals from noisy acceleration data. *International Journal of Applied Electromagnetics and Mechanics*, 2003, 18(1-3): 149–163.

[11] J. Medrano, F. Yumbla, S. Jeong, I. Choi, Y. Park, E. Auh, and H. Moon, Jerk estimation for quadrotor based on differential flatness, in *Proceedings of 2020 17th International Conference on Ubiquitous Robots (UR)*, 2020: 99–104.

[12] E. Tal and S. Karaman, Accurate tracking of aggressive quadrotor trajectories using incremental nonlinear dynamic inversion and differential flatness. *IEEE Transactions on Control Systems Technology*, 2020, 29(3): 1203–1218.

[13] G. R. Duan, High-order fully actuated system approaches: Part III. Robust control and high-order backstepping. *International Journal of Systems Science*, 2021, 52(5): 952–971.

[14] S. Krafes, Z. Chalh, and A. Saka, A review on the control of second order underactuated mechanical systems. *Complexity*, 2018, 2018(1): 9573514.

[15] W. Ren, G. R. Duan, and H. Kong, A Fully Actuated System Approach to Interval Observer Design with Applications in Fault Detection, in *2024 3rd Conference on Fully Actuated System Theory and Applications (FASTA)*, 2024: 571–576.